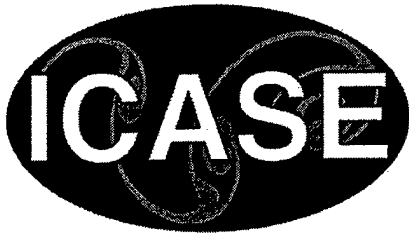


NASA/CR-2000-209854
ICASE Report No. 2000-6



An Accurate Curved Boundary Treatment in the Lattice Boltzmann Method

Renwei Mei
University of Florida, Gainesville, Florida

Li-Shi Luo
ICASE, Hampton, Virginia

Wei Shyy
University of Florida, Gainesville, Florida

Institute for Computer Applications in Science and Engineering
NASA Langley Research Center
Hampton, VA
Operated by Universities Space Research Association



National Aeronautics and
Space Administration

Langley Research Center
Hampton, Virginia 23681-2199

Prepared for Langley Research Center
under Contract NAS1-97046

February 2000

DISTRIBUTION STATEMENT A
Approved for Public Release
Distribution Unlimited

DTIC QUALITY INSPECTED 3

20000315 053

AN ACCURATE CURVED BOUNDARY TREATMENT IN THE LATTICE BOLTZMANN METHOD

RENWEI MEI*, LI-SHI LUO†, AND WEI SHYY‡

Abstract. The lattice Boltzmann equation (LBE) is an alternative kinetic method capable of solving hydrodynamics for various systems. Major advantages of the method are owing to the fact that the solution for the particle distribution functions is explicit, easy to implement, and natural to parallelize. Because the method often uses uniform regular Cartesian lattices in space, curved boundaries are often approximated by a series of stairs that leads to reduction in computational accuracy. In this work, a second-order accurate treatment of boundary condition in the LBE method is developed for a curved boundary. The proposed treatment of the curved boundaries is an improvement of a scheme due to Filippova and Hänel. The proposed treatment for curved boundaries is tested against several flow problems: 2-D channel flows with constant and oscillating pressure gradients for which analytic solutions are known, flow due to an impulsively started wall, lid-driven square cavity flow, and uniform flow over a column of circular cylinders. The second-order accuracy is observed with solid boundary arbitrarily placed between lattice nodes. The proposed boundary condition has well behaved stability characteristics when the relaxation time is close to $1/2$, the zero limit of viscosity. The improvement can make a substantial contribution toward simulating practical fluid flow problems using the lattice Boltzmann method.

Key words. kinetic method, lattice Boltzmann equation, Navier-Stokes equation, second order boundary conditions

Subject classification. Fluid Mechanics

1. Introduction. There has been a rapid progress in developing and employing the method of the lattice Boltzmann equation (LBE) [24, 20, 5] as an alternative computational technique for solving complex fluid dynamic problems (see the comprehensive reviews in [3, 6]). In a traditional method for computational fluid dynamics (CFD), the macroscopic variables, such as velocity \mathbf{u} and pressure p , are obtained by solving the Navier-Stokes (NS) equations [28, 9, 31]. The lattice Boltzmann equation approximates the kinetic equation for the single particle (mass) distribution function $f(\mathbf{x}, \boldsymbol{\xi}, t)$ on the mesoscopic level, such as the Boltzmann equation with the single relaxation time approximation [4]:

$$(1.1) \quad \partial_t f + \boldsymbol{\xi} \cdot \nabla f = -\frac{1}{\lambda} [f - f^{(0)}],$$

where $\boldsymbol{\xi}$ is the particle velocity, $f^{(0)}$ is the equilibrium distribution function (the Maxwell-Boltzmann distribution function), and λ is the relaxation time. The right hand side (RHS) of Eq. (1.1) models the effect of

*Department of Aerospace Engineering, Mechanics and Engineering Science, University of Florida, Gainesville, FL 32611-6250 (email address: rwm@aero.ufl.edu).

†Institute for Computer Applications in Science and Engineering, Mail Stop 132C, NASA Langley Research Center, 3 West Reid Street, Building 1152, Hampton, VA 23681-2199 (email address: luo@icase.edu). This research was supported by the National Aeronautics and Space Administration under NASA Contract No. NAS1-97046 while the author was in residence at the Institute for Computer Applications in Science and Engineering (ICASE), NASA Langley Research Center, Hampton, VA 23681-2199.

‡Department of Aerospace Engineering, Mechanics and Engineering Science, University of Florida, Gainesville, FL 32611-6250 (email address: wss@tiger.aero.ufl.edu).

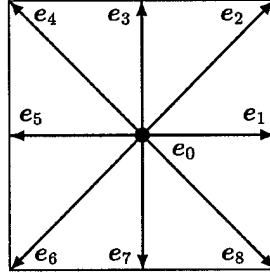


FIG. 1. Two-dimensional 9-velocity (or 9-bit) lattice.

the fluid viscosity on the molecular level through the collision (relaxation) process. The macroscopic quantities (such as mass density ρ and momentum density ρu) are the hydrodynamic moments of the distribution function f :

$$(1.2a) \quad \rho = \int f(x, \xi, t) d\xi,$$

$$(1.2b) \quad \rho u = \int \xi f(x, \xi, t) d\xi.$$

It has been shown that the velocity space ξ can be discretized into a finite set of points $\{\xi_\alpha\}$ without affecting the conservation laws [14, 15, 1]. In the discretized velocity space the Boltzmann equation (1.1) becomes

$$(1.3) \quad \partial_t f_\alpha + \xi_\alpha \cdot \nabla f = -\frac{1}{\lambda} [f_\alpha - f_\alpha^{(eq)}], \quad (\alpha = 0, 1, 2, \dots, 8 \text{ for 2-D}),$$

for the distribution function of discrete velocities $f_\alpha(x, t) \equiv f(x, \xi_\alpha, t)$. The equilibrium distribution function, $f_\alpha^{(eq)}$, and the discrete velocity set $\{\xi_\alpha\}$ can be derived explicitly [14, 15, 1].

For 2-D square lattice shown in Fig. 1, we use $\{e_\alpha\}$ to denote the discrete velocity set, and we have [29]:

$$(1.4) \quad e_\alpha = \begin{cases} (0, 0), & \alpha = 0, \\ (\cos[(\alpha - 1)\pi/4], \sin[(\alpha - 1)\pi/4]) c, & \alpha = 1, 3, 5, 7, \\ (\cos[(\alpha - 1)\pi/4], \sin[(\alpha - 1)\pi/4]) \sqrt{2}c, & \alpha = 2, 4, 6, 8, \end{cases}$$

where $c = \delta_x/\delta_t$, δ_x and δ_t are the lattice constant and the time step size, respectively, and

$$(1.5) \quad f_\alpha^{(eq)} = w_\alpha \rho \left[1 + \frac{3}{c^2} e_\alpha \cdot u + \frac{9}{2c^4} (e_\alpha \cdot u)^2 - \frac{3}{2c^2} u \cdot u \right],$$

where

$$(1.6) \quad w_\alpha = \begin{cases} \frac{4}{9}, & \alpha = 0, \\ \frac{1}{9}, & \alpha = 1, 3, 5, 7, \\ \frac{1}{36}, & \alpha = 2, 4, 6, 8. \end{cases}$$

With the discretized velocity space, the hydrodynamic moments are given by:

$$(1.7a) \quad \rho = \sum_\alpha f_\alpha = \sum_\alpha f_\alpha^{(eq)},$$

$$(1.7b) \quad \rho u = \sum_\alpha e_\alpha f_\alpha = \sum_\alpha e_\alpha f_\alpha^{(eq)}.$$

The speed of sound of this model is $c_s = c/\sqrt{3}$, and the equation of state is that of an ideal gas,

$$(1.8) \quad p = c_s^2 \rho.$$

Equation (1.3) is one of numerous ways to model the transport equation of f , Eq. (1.1).

Based on the Chapman-Enskog analysis, the solution for $f_\alpha(\mathbf{x}, t)$ may be expanded in the form of

$$(1.9) \quad f_\alpha(\mathbf{x}, t) = f_\alpha^{(\text{eq})}(\mathbf{x}, t) + \epsilon f_\alpha^{(1)}(\mathbf{x}, t) + \dots,$$

where $\epsilon = \text{Kn}$ is the formal expansion parameter and Kn is the Knudsen number, which is the ratio between the mean free path and macroscopic flow characteristic length. Substitution of Eq. (1.9) into Eq. (1.3) with a factor $1/\epsilon$ in the collision term leads to

$$(1.10) \quad f_\alpha^{(1)}(\mathbf{x}, t) = -\lambda \left[\partial_t f_\alpha^{(\text{eq})}(\mathbf{x}, t) + \mathbf{e}_\alpha \cdot \nabla f_\alpha^{(\text{eq})}(\mathbf{x}, t) \right].$$

Proceeding with the Chapman-Enskog analysis, it can be shown that the Euler equations can be recovered from the solution for $f_\alpha^{(\text{eq})}$, and the NS equations are recovered in the near incompressible limit (*i.e.*, the Mach number $M = |\mathbf{u}|/c_s \ll 1$) by the first two terms in Eq. (1.9). The viscosity of the fluid is

$$(1.11) \quad \nu = c_s^2 \lambda.$$

Equation (1.3) can be further discretized in space and time. The completely discretized form of Eq. (1.3), with the time step δ_t and space step $\mathbf{e}_\alpha \delta_t$, is:

$$(1.12) \quad f_\alpha(\mathbf{x}_i + \mathbf{e}_\alpha \delta_t, t + \delta_t) - f_\alpha(\mathbf{x}_i, t) = -\frac{1}{\tau} [f_\alpha(\mathbf{x}_i, t) - f_\alpha^{(\text{eq})}(\mathbf{x}_i, t)],$$

where $\tau = \lambda/\delta_t$, and \mathbf{x}_i is a point in the discretized physical space. The above equation is the lattice Boltzmann equation [24, 20, 5] with Bhatnagar-Gross-Krook (BGK) approximation [4]. The left-hand side (LHS) of Eq. (1.12) is physically a streaming process for particles while the RHS models the collisions through relaxation.

Although the lattice Boltzmann equation historically originates from the lattice gas cellular automata [10, 30], it is indeed a special finite difference form of the continuous Boltzmann kinetic equation, *i.e.*, the LHS of Eq. (1.1) is discretized along the direction of the characteristic line with discretization of phase space and time tied together [14, 15]. The leading order truncation error of such a discretization is then taken into account exactly by modifying the viscosity in the NS equation derived from Eq. (1.12) to

$$(1.13) \quad \nu = c_s^2 \delta_t \left(\tau - \frac{1}{2} \right).$$

The positivity of the viscosity thus requires that $\tau > 1/2$. The lattice Boltzmann scheme consists of two computational steps:

$$(1.14a) \quad \text{Collision:} \quad \tilde{f}_\alpha(\mathbf{x}_i, t) = f_\alpha(\mathbf{x}_i, t) - \frac{1}{\tau} [f_\alpha(\mathbf{x}_i, t) - f_\alpha^{(\text{eq})}(\mathbf{x}_i, t)],$$

$$(1.14b) \quad \text{Streaming:} \quad f_\alpha(\mathbf{x}_i + \mathbf{e}_\alpha \delta_t, t + \delta_t) = \tilde{f}_\alpha(\mathbf{x}_i, t),$$

where f_α and \tilde{f}_α denote pre- and post-collision state of the distribution function, respectively. The advantages of solving the lattice Boltzmann equation over the NS equations can now be seen. In the kinetic equation for f_α given by Eq. (1.3), the advection operator is linear in the phase space whereas the convection term is nonlinear in the NS equation. In traditional CFD methods, the pressure is typically obtained by solving the Poisson or Poisson-like equation derived from the incompressible NS equations that can be time consuming. In the LBE method, the pressure is obtained through an extremely simple equation of state $p = c_s^2 \rho$. This is an appealing feature of the LBE method. The discretized Eq. (1.12) for f_α is explicit in form, easy to

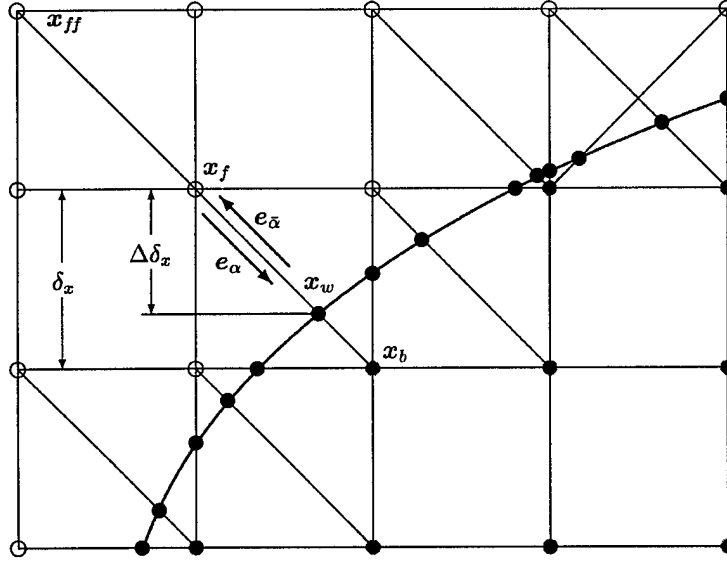


FIG. 2. Layout of the regularly spaced lattices and curved wall boundary. The thick curve marks the boundary location. The solid circles (•) mark the positions where particle-boundary collision occurs. The empty (o) and shaded (•) circles are fluid sites and solid sites, respectively.

implement, and natural to parallelize. The collision step is completely local. The streaming step takes very little computational effort at every time step.

However, unlike solving the NS equations for which the non-slip condition for u on a solid wall is satisfied at the macroscopic level, there is no corresponding, physically based boundary condition for f_α on a solid wall at the mesoscopic level. For a lattice node located on the fluid side at x_f , as illustrated in Fig. 2, Eq. (1.14b) clearly indicates a need for the information of at x_b on the solid side. Therefore all the effort in the previous treatment of the boundary conditions in the LBE models is much focused on the calculation of \tilde{f}_α moving from the wall into the fluid region. In previous works of the LBE, the most often used boundary condition on the wall is the so-called bounce-back scheme [32, 11, 19]. In the bounce-back scheme, after a particle distribution f_α streams from a fluid node at x_f to a boundary node at x_b along the direction of e_α , the particle distribution f_α scatters back to the node x_f along the direction of $e_{\bar{\alpha}} (= -e_\alpha)$ as $\tilde{f}_{\bar{\alpha}}$. Since the wall position x_w was forced to be located at x_b , this is referred to as bounce-back on the node (BBN) [2]. However, a finite slip velocity at the stationary wall exists [22, 19] and the accuracy for the flow field is thus degraded due to the inaccuracy of the boundary conditions [11]. In simulating suspension flows using the LBE method, Ladd placed the solid walls in the middle between the lattice nodes [21]. This is referred to as bounce-back on the link (BBL). It has been shown that the BBL scheme gives second-order accurate result for straight walls [33, 19]. Noble *et al.* developed a second-order accurate boundary condition to compute $\tilde{f}_{\bar{\alpha}}$ but it is only applicable to straight walls in triangular lattice space [27]. He *et al.* generalized the scheme of Noble *et al.* to arbitrary lattice [19]. Chen *et al.* placed the wall on the lattice node so that x_b is one lattice inside the wall [7]. They used an extrapolation of f_α on the fluid side (including the wall node) to obtain f_α at x_b . Zou and He proposed to apply the BBL scheme only for the non-equilibrium part of f_α at the wall [33].

For a curved geometry, the use of BBL requires approximation of the curved solid boundary by a series of stair steps. The geometric integrity cannot be preserved by such an approximation. For high Reynolds

number flows, the integrity of geometry is important since the vorticity generation and stress distributions are sensitive to the geometrical resolution. To this end, He and Luo proposed to use the LBE with nonuniform grid with second order interpolations [14, 17, 18]. He and Doolen further applied the interpolation to the LBE with curvilinear coordinates or body-fitted coordinates [13]. Mei and Shyy solved Eq. (1.3) in curvilinear coordinates using finite difference method [25]. While the wall geometry is accurately preserved in body-fitted coordinates, the flexibility to handle complex geometries is maintained by using the numerical grid generation techniques common to the Navier-Stokes solvers. It should be noted that perhaps the most profound and rigorous theoretical treatment of the boundary condition along the wall is given by Ginzbourg and d'Humières [12]. The scheme proposed by Ginzbourg and d'Humières is local and accurate up to second order in Chapman-Enskog expansion. However this work has not attracted sufficient attention because its implementation is not as easy as the bounce-back scheme.

In this work, a robust, second-order accurate treatment for the distribution function f_α near a curved boundary is developed based on the method recently proposed by Filippova and Hänel (hereinafter referred as FH) [8]. In Ref. [8], the boundary condition for f_α on the solid side is evaluated using Eq. (1.3) for f_α , and the Taylor series expansion in both space and time for f_α near the wall. FH reported numerical results for a uniform flow over a cylinder [8]. However, it is found in this work that when tested in a pressure driven channel flow (see implementation and discussions in Section 2) there is a strong boundary condition induced instability when the distance from the wall to the first lattice on the fluid side is less than half of the lattice size.

Using the Taylor series expansion for the velocity u near the wall, a new treatment for f_α near a curved wall is proposed in this work. While maintaining a second-order accuracy of the solution in handling curved walls, the computational stability is improved so that lower viscosity, or higher Reynolds number, can be attained in the LBE simulations. The new boundary condition treatment is tested systematically to assess the temporal and spatial accuracy and robustness in 2-D channel flow with constant and oscillating pressure gradients, flow due to an impulsively started wall, lid-driven square cavity flow, and flow over a column of circular cylinders. Detailed comparisons for the flow field are made with either analytic solutions or well resolved numerical solutions of the Navier-Stokes equations by using finite difference method. The improved boundary treatment represents a significant step towards solving practically relevant flow problems using the LBE method.

2. Formulation for the Improved Boundary Condition. Filippova and Hänel considered a curved boundary lying between the lattice nodes of spacing δ_x , as illustrated in Fig. 2, and briefly presented the derivation of their scheme for the treatment of curved boundary in Ref. [8]. However, they did not offer a thorough explanation to justify the theoretical basis of their method. It is instructive to first re-examine their derivation thoroughly. Based on the insight gained, an improved boundary treatment is then proposed.

2.1. Re-examination of and comments on Filippova-Hänel's treatment. The macroscopic flow has a characteristic length of L . The lattice nodes on the solid and fluid side are denoted as x_b and x_f , respectively, in Fig. 2. The filled small circles on the boundary, x_w , denote the intersections of the wall with various lattice links. The boundary velocity at x_w , the intersection with the wall on the link between x_b and x_f , is u_w . The fraction of the intersected link in the fluid region is Δ , as illustrated in Fig. 2, that is:

$$(2.1) \quad \Delta = \frac{|x_f - x_w|}{|x_f - x_b|}.$$

Obviously, $0 \leq \Delta \leq 1$ and the horizontal or vertical distance between x_f and x_w is $\Delta \cdot \delta_x$ on the square lattice. Suppose the particle momentum moving from x_f to x_b is e_α and the reversed one from x_b to x_f is

$e_{\bar{\alpha}} = -e_{\alpha}$. After the collision step, \tilde{f}_{α} on the fluid side is known, but not on the solid side. (Hereafter we shall use $e_{\bar{\alpha}}$ and $f_{\bar{\alpha}}$ to denote the velocity and the distribution function coming from a solid node to a fluid node, and $f_{\bar{\alpha}}$ is the unknown to be computed.) To finish the streaming step,

$$(2.2) \quad f_{\bar{\alpha}}(x_f = x_b + e_{\bar{\alpha}}\delta_t, t + \delta_t) = \tilde{f}_{\bar{\alpha}}(x_b, t),$$

it is clear that $\tilde{f}_{\bar{\alpha}}(x_b, t)$ is needed. To construct $\tilde{f}_{\bar{\alpha}}(x_b, t)$ based upon some known information in the surrounding, Filippova and Hänel essentially proposed to use the following linear interpolation [8]:

$$(2.3) \quad \tilde{f}_{\bar{\alpha}}(x_b, t) = (1 - \chi)\tilde{f}_{\alpha}(x_f, t) + \chi f_{\alpha}^{(*)}(x_b, t) - 2w_{\alpha}\rho\frac{3}{c^2}(e_{\bar{\alpha}} \cdot u_w),$$

where $u_w \equiv u(x_w, t)$ is the velocity at wall, χ is the weighting factor (to be determined) that controls the linear interpolation (or extrapolation) between $\tilde{f}_{\alpha}(x_f, t)$ and $f_{\alpha}^{(*)}(x_b, t)$, a fictitious equilibrium distribution function given by

$$(2.4) \quad f_{\alpha}^{(*)}(x_b, t) = w_{\alpha}\rho(x_f, t) \left[1 + \frac{3}{c^2}e_{\alpha} \cdot u_{bf} + \frac{9}{2c^4}(e_{\alpha} \cdot u_f)^2 - \frac{3}{2c^2}u_f \cdot u_f \right].$$

In the above equation, $u_f \equiv u(x_f, t)$ is the fluid velocity near the wall and u_{bf} is to be determined later. It should be emphasized here that the weighting factor χ depends on how u_{bf} is chosen. However, the choice of u_{bf} is not unique. For example, either $u_{bf} = u_f$ or a linear extrapolation using $u_{bf} = [(\Delta - 1)u_f + u_w]/\Delta$ appears reasonable at this stage.

To determine χ in Eq. (2.3), FH considered flows under the condition

$$(2.5) \quad \frac{L}{cT} \ll 1,$$

i.e., the flow has an intrinsic characteristic time scale T that is much larger than the advection time on the lattice scale, L/c . This “slow-flow” condition enabled FH to approximate $f_{\bar{\alpha}}(x_f, t + \delta_t)$ in Eq. (2.2) by $f_{\bar{\alpha}}(x_f, t)$,

$$(2.6) \quad f_{\bar{\alpha}}(x_f = x_b + e_{\bar{\alpha}}\delta_t, t + \delta_t) = f_{\bar{\alpha}}(x_f, t) + \delta_t \partial_t f_{\bar{\alpha}} + \dots$$

For the purpose of the order-of-magnitude estimate, it is seen that $O(\partial_t f_{\bar{\alpha}}) = O(f_{\bar{\alpha}}/T)$ so that

$$(2.7) \quad f_{\bar{\alpha}}(x_f, t + \delta_t) = f_{\bar{\alpha}}(x_f, t) \left[1 + O\left(\frac{\delta_t}{T}\right) \right] = f_{\bar{\alpha}}(x_f, t) \left[1 + O\left(\frac{\delta_x}{L} \frac{L}{cT}\right) \right] \approx f_{\bar{\alpha}}(x_f, t).$$

It is noted that under condition (2.5) the neglected terms are of $O(\frac{\delta_x}{L} \frac{L}{cT})$ which are much smaller than the $O(\frac{\delta_x}{L})$ terms of the present interest [in deriving an accurate boundary condition for $\tilde{f}_{\bar{\alpha}}(x_b, t)$]. Applying the Chapman-Enskog expansion in the form given by Eqs. (1.9) and (1.10) and invoking the “slow flow” approximation defined by Eq. (2.5), one obtains

$$(2.8) \quad \begin{aligned} f_{\bar{\alpha}}(x_f, t) &= f_{\bar{\alpha}}^{(\text{eq})}(x_f, t) - \lambda \left[\partial_t f_{\bar{\alpha}}^{(\text{eq})} + e_{\bar{\alpha}} \cdot \nabla f_{\bar{\alpha}}^{(\text{eq})} \right] + \dots \\ &\approx f_{\bar{\alpha}}^{(\text{eq})}(x_f, t) - \lambda e_{\bar{\alpha}} \cdot \nabla f_{\bar{\alpha}}^{(\text{eq})} + \dots \end{aligned}$$

For $f_{\bar{\alpha}}^{(\text{eq})}$ given by Eq. (1.5), the leading order term in $\nabla f_{\bar{\alpha}}^{(\text{eq})}$ is given by $3w_{\alpha}\rho\nabla(u \cdot e_{\bar{\alpha}})/c^2$ since the rest are higher order terms in the near incompressible flow limit. Noticing that $\lambda = \tau\delta_t$, Eq. (2.8) becomes

$$(2.9) \quad \begin{aligned} f_{\bar{\alpha}}(x_f, t) &\approx f_{\bar{\alpha}}^{(\text{eq})}(x_f, t) - 3w_{\alpha}\rho\tau\delta_t\frac{1}{c^2}e_{\bar{\alpha}} \cdot \nabla(u_f \cdot e_{\bar{\alpha}}) \\ &= f_{\bar{\alpha}}^{(\text{eq})}(x_f, t) - 6w_{\alpha}\rho\frac{1}{c^2}u_f \cdot e_{\alpha} - 3w_{\alpha}\rho\tau\delta_t\frac{1}{c^2}e_{\bar{\alpha}} \cdot \nabla(u_f \cdot e_{\bar{\alpha}}), \end{aligned}$$

which approximates the LHS of Eq. (2.2). To expand the RHS of Eq. (2.2) in terms of the small computational parameter

$$(2.10) \quad \frac{\delta_x}{L} = \frac{c\delta_t}{L} \ll 1,$$

it is first noted that $f_\alpha^{(*)}(\mathbf{x}_b, t)$ in Eq. (2.4) can be expressed as

$$(2.11) \quad f_\alpha^{(*)}(\mathbf{x}_b, t) = f_\alpha^{(\text{eq})}(\mathbf{x}_b, t) + w_\alpha \rho \frac{3}{c^2} \mathbf{e}_\alpha \cdot (\mathbf{u}_{bf} - \mathbf{u}_f),$$

so that the RHS of Eq. (2.2), or Eq. (2.3), can be rewritten as

$$(2.12) \quad \begin{aligned} \tilde{f}_\alpha(\mathbf{x}_f, t) &\approx f_\alpha^{(\text{eq})}(\mathbf{x}_f, t) + (1 - \chi)(1 - 1/\tau)f_\alpha^{(1)}(\mathbf{x}_f, t) + w_\alpha \rho \frac{3}{c^2} \mathbf{e}_\alpha \cdot (\chi \mathbf{u}_{bf} - \chi \mathbf{u}_f - 2\mathbf{u}_w) \\ &= f_\alpha^{(\text{eq})}(\mathbf{x}_f, t) - (1 - \chi)(\tau - 1)\delta_t w_\alpha \rho \frac{3}{c^2} \mathbf{e}_\alpha \cdot \nabla \mathbf{u}_f \cdot \mathbf{e}_\alpha + w_\alpha \rho \frac{3}{c^2} \mathbf{e}_\alpha \cdot (\chi \mathbf{u}_{bf} - \chi \mathbf{u}_f - 2\mathbf{u}_w). \end{aligned}$$

Based on linear interpolation, $\mathbf{u}_{bf} \approx [(\Delta - 1)\mathbf{u}_f + \mathbf{u}_w]/\Delta$, expanding the velocity \mathbf{u}_w at \mathbf{x}_f near the wall (\mathbf{x}_w) using Taylor series, i.e., $\mathbf{u}_w = \mathbf{u}_f + \Delta \delta_t \mathbf{e}_\alpha \cdot \nabla \mathbf{u}_f$, one obtains $\mathbf{u}_{bf} - \mathbf{u}_f \approx \delta_t \mathbf{e}_\alpha \cdot \nabla \mathbf{u}$. Noticing that $(\mathbf{x}_b - \mathbf{x}_f) = \mathbf{e}_\alpha \delta_t$, and equating Eqs. (2.9) and (2.12) and matching terms linear in δ_t results in $\chi = (2\Delta - 1)/\tau$. For $\mathbf{u}_{bf} = \mathbf{u}_f$, we have $\mathbf{u}_{bf} - \mathbf{u}_f = 0$ in Eq. (2.12). Matching to $O(\delta_t)$ then requires $\chi = (2\Delta - 1)/(\tau - 1)$. FH found that $\mathbf{u}_{bf} = [(\Delta - 1)\mathbf{u}_f + \mathbf{u}_w]/\Delta$ gives computationally stable results only for $\Delta \geq 1/2$. Hence, they proposed that

$$(2.13) \quad \mathbf{u}_{bf} = \frac{1}{\Delta}(\Delta - 1)\mathbf{u}_f + \frac{1}{\Delta}\mathbf{u}_w, \quad \text{and} \quad \chi = \frac{(2\Delta - 1)}{\tau}, \quad \text{for} \quad \Delta \geq \frac{1}{2},$$

and

$$(2.14) \quad \mathbf{u}_{bf} = \mathbf{u}_f, \quad \text{and} \quad \chi = \frac{(2\Delta - 1)}{(\tau - 1)}, \quad \text{for} \quad \Delta < \frac{1}{2}.$$

To recapitulate, there are three independent assumptions that have been made in the foregoing derivation. They are: (i) the Chapman-Enskog expansion in the form given by Eqs. (1.9) and (1.10) is valid; (ii) the intrinsic time scale of the unsteady flow must be much large compared to the advection time on the lattice scale given by Eq. (2.5); and (iii) the lattice spacing must be small compared to the characteristic length scale of the flow as given by Eq. (2.10) so that the Taylor series expansion for the velocity field near the wall is valid. There have been a large number of papers in the existing literature regarding the validity and usefulness of the Chapman-Enskog analysis for the solution of the Boltzmann equation. The “slow flow” condition is introduced to simplify the derivation of the boundary condition for f_α ; the implication of this assumption will be briefly addressed later in comparing the computational results with that based on the conventional bounce-back scheme. The last assumption is a typical computational resolution requirement.

Equation (2.3) is essentially a linear interpolation (or extrapolation) and is used continuously in the computation. When the weighting factor χ becomes too large, instability may develop. For $1 > \Delta \geq 1/2$, $|\chi| = |2\Delta - 1|/\tau$ is always less than 2 because the positivity of the viscosity in the LBE scheme requires $\tau > 1/2$. For $0 \leq \Delta < 1/2$, $|\chi| = |(2\Delta - 1)/(\tau - 1)|$, and it may become too large when τ is close to 1. To illustrate this point, a fully developed pressure driven 2-D channel flow is considered. The grid arrangement is shown in Fig. 3. For steady flow, a constant pressure gradient ∇p along the x -direction is applied and can be treated as a body force. This is included [23] after the collision step by

$$(2.15) \quad \tilde{f}_\alpha(\mathbf{x}_i, t) = f_\alpha(\mathbf{x}_i, t) + w_\alpha \delta_t \frac{3}{c^2} \frac{dp}{dx} \mathbf{e}_\alpha \cdot \hat{\mathbf{x}},$$

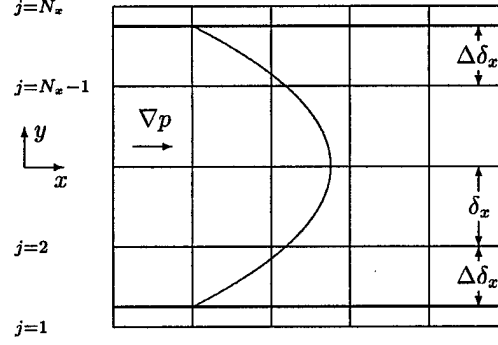


FIG. 3. Lattice configuration in channel flow simulations with an arbitrary Δ .

where \hat{x} is the unit vector along the x -axis. The boundary condition for $\tilde{f}_\alpha(x_i, t)$ on the wall follows those given by Eqs. (2.3), (2.4), (2.13), and (2.14). At the inlet ($i = 1$) and exit ($i = N_x$, in which N_x is the number of lattices in the x -direction) the following is imposed,

$$(2.16) \quad f_\alpha(i = 1, j) = f_\alpha(i = 2, j),$$

$$(2.17) \quad f_\alpha(i = N_x, j) = f_\alpha(i = N_x - 1, j).$$

With Eq. (2.16), the velocity profile at the inlet, $u_x(i = 2, j)$, is not needed. Instead, the fully developed velocity profile is sought as part of the solutions. In this part of the investigation, $N_y = 35$ is used. The exact solution for the velocity profile [given by Eq. (3.1)] is used as the velocity initial condition which differs from the final steady state solution due to numerical errors. The equilibrium distribution function $f_\alpha^{(eq)}$ based on the exact solution for the velocity profile is used as the initial condition for f_α . The pressure gradient is set to $\frac{dp}{dx} = -1.0 \times 10^{-6}$. All computations are carried out in double precision.

For $\Delta < 1/2$, it is found that the computation is unstable for certain range of values of τ . In Figure 4, solid curves are the stability-instability boundaries for the fully developed channel flow in the (Δ, τ) space obtained from a large number of computations. For $\Delta < 0.2$, the computation becomes unstable when $\tau < 1$. The large instability region is an apparent source of concern for FH's scheme when $\Delta < 1/2$ since lower viscosity can only be achieved when τ is close to $1/2$.

One may speculate that the instability in the above example results from the lack of specifying an inlet velocity profile, $u_x(y)$, or due to the extrapolation of f_α at the inlet given by Eq. (2.16). To examine this possibility, a channel flow entrance problem is considered. Uniform velocity profiles, $u_x(y) = -(H/12\rho\nu)(dp/dx)$ and $u_y(y) = 0$ in which H is the channel height, are specified at $i = 1.5$ (half way between the first and second lattices) and the distribution functions $f_\alpha(i = 1, j)$ for $\alpha = 1, 2$, and 8 are obtained using Eq. (2.3) with $\chi = 0$ in accordance with $\Delta = 1/2$ at $i = 1.5$. The boundary conditions on the wall are based on Eqs. (2.3), (2.4), (2.13), and (2.14). The exit boundary condition for f_α 's is given by Eq. (2.17). Hence the extrapolation for f_α at the inlet is completely eliminated and the velocity profiles at the inlet are exactly given. Two types of initial conditions are used. Whenever possible, the equilibrium distribution functions corresponding to the uniform inlet velocity are specified at $t = 0$ throughout the flow field. This works for relatively larger values of τ . However, instability can be encountered when τ is considerably larger than the upper solid curve shown in Fig. 4 for the same value of Δ ($< 1/2$). A second type of initial condition is thus implemented. A converged solution at a relatively large value of τ is used as the initial condition for a

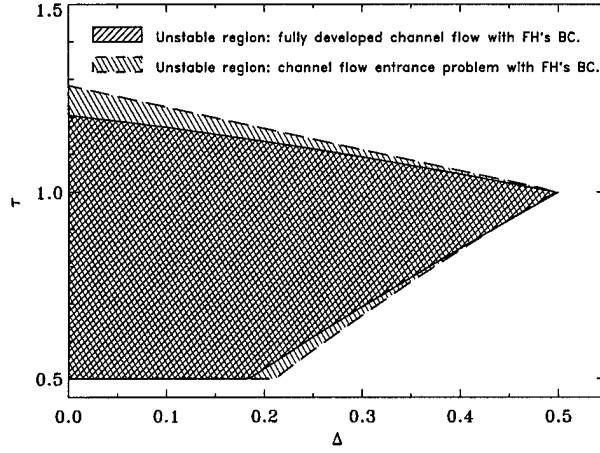


FIG. 4. Regions of instability in the LBE computation for channel flows using FH's boundary condition, Eqs. (2.3), (2.4), (2.13), and (2.14), with $\Delta < 1/2$. The instability region for the fully developed 2-D channel flow (enclosed by solid curves) is slightly smaller than the instability region for the 2-D channel flow entrance problem (enclosed by dashed curves).

smaller value of τ . The value of τ is incrementally decreased to obtain the converged solutions for the new, smaller values of τ . When the actual instability region is approached, the increment in τ is maintained as small as 0.01 or 0.005. In the computation, $\frac{dp}{dx} = -1.0 \times 10^{-6}$, $N_y = 35$, and $N_x = 65$ are used. When the Reynolds number is low (due to the use of the small pressure gradient and larger τ), the exit velocity profile is very close to the exact solution corresponding to the fully developed channel flow which validates the solution procedure.

The stability-instability boundaries for the channel flow entrance problem obtained through a large number of computations (dashed curves) are also shown in Fig. 4. It is noted that the stability-instability boundaries for the channel flow entrance problem are very similar to, and slightly larger than, that for the fully developed channel flow despite the significant difference in the inlet boundary condition. Thus the source of the instability must be a result mainly due to the implementation of the solid wall condition. An alternative scheme must be developed to overcome this shortcoming.

2.2. Improved treatment for curved boundary. We realize that the flexibility in the construction of is the key to achieve an improved computational stability as well as accuracy. Since $\chi = (2\Delta - 1)/(\tau - 1)$ given by Eq. (2.14) leads to a larger value of χ when τ is close to 1, it is desirable to reduce the magnitude of χ by increasing the magnitude of the denominator in the expression for χ . For $\Delta \geq 1/2$, u_{bf} is the fictitious fluid velocity inside the solid and the denominator for χ is τ . For $\Delta < 1/2$, u_{bf} was chosen by FH to be u_f which is the fluid velocity at x_f and it leads to $(\tau - 1)$ in the denominator for χ . Thus, we propose to use Eq. (2.13) for $\Delta \geq 1/2$ and use

$$(2.18) \quad u_{bf} = u_{ff} = u(x_f + e_{\bar{\alpha}}\delta_t, t), \quad \text{for } \Delta < \frac{1}{2}.$$

Thus

$$(2.19) \quad u_{bf} - u_f = u(x_f + e_{\bar{\alpha}}\delta_t, t) - u(x_f, t) = -\delta_t \nabla u_f \cdot e_{\bar{\alpha}}.$$

This requires

$$(2.20) \quad -\tau(1 - \chi)(1 - 1/\tau) - \chi = 2\Delta - \tau$$

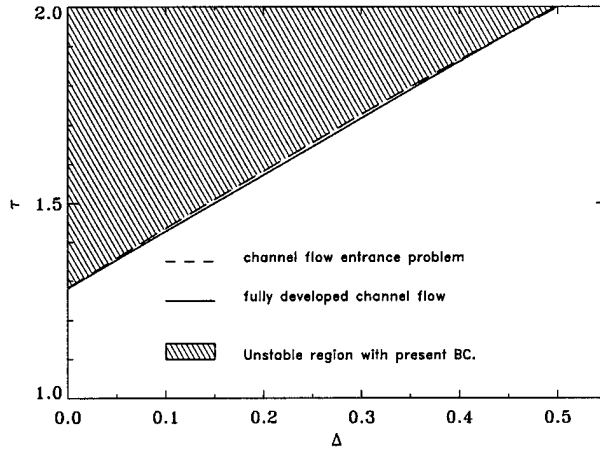


FIG. 5. Regions of stability and instability in the LBE computation for channel flow using the present boundary condition, Eqs. (2.3), (2.4), (2.13), (2.18), and (2.21), with $\Delta < 1/2$, similar to FIG. 4. The instability region for the fully developed 2-D channel flow (above the solid curve) is almost the same as the instability region for the 2-D channel flow entrance problem (above the dashed curve).

to match the $O(\delta_t)$ terms in equating Eqs. (2.9) and (2.12). Hence

$$(2.21) \quad \chi = \frac{(2\Delta - 1)}{(\tau - 2)}, \quad \text{for } \Delta < \frac{1}{2}.$$

To test the improvement in the stability, the steady state, fully developed, pressure driven 2-D channel flow is again considered. Eqs. (2.18) and (2.21) are used in lieu of Eq. (2.14). The rest of the implementation is exactly the same as described in the previous section. The solid curve in Fig. 5 shows the stability-instability boundary in the (Δ, τ) space for the fully developed channel flow. By comparing Fig. 5 with Fig. 4, the improvement in the stability of the present treatment for this case is clearly seen. The present treatment moves the instability region around $\tau = 1$ caused by FH's boundary condition upward in the parameter space (Δ, τ) to the region around $\tau = 2$. This would enable us to use τ in the interval $(0.5, 1.2]$ for small viscosity.

For the channel flow entrance problem, boundary conditions at the inlet and exit and the procedure for specifying the initial conditions are the same as described in the last section. Eqs. (2.18) and (2.21) are used to replace Eq. (2.14) for the solid wall. The stability-instability boundary in the (Δ, τ) space for the entrance flow problem is shown by the dashed curve in Fig. 5. Close agreement between the stability-instability boundaries for the two cases in Fig. 5 suggests that the improvement in the computational stability is not related to the treatment of the inlet boundary conditions. The improvement results rather from the different treatment in the solid wall boundary condition. One advantage of the present treatment of solid wall is its insensitivity to other boundary conditions such as inlet and outlet boundary condition in channel flows, as indicated by the results shown in Fig. 5. The instability in the present treatment is mainly due the denominator $(\tau - 2)$ in Eq. (2.21). A direct consequence of this improvement is that lower values of τ , or lower viscosity ν , can now be used.

As one may speculate at this point that $u(x_f + 2e_{\alpha}\delta_t, t)$ can also be used for u_{bf} when $\Delta < 1/2$. This would further improve the stability since $\chi = (2\Delta - 1)/(\tau - 3)$. This is correct in principle. However, since the use of u_f as u_{bf} already allows the use of τ whose value is close to $1/2$, there is little practical need to use u_f that is too far away from the wall.

For transient flows, a second-order extrapolation can be used for

$$(2.22) \quad \begin{aligned} u_{bf} &= \frac{\Delta - 1}{\Delta} u_f + \frac{1}{\Delta} u_w + \frac{1 - \Delta}{\Delta(1 + \Delta)} [u_w - (1 + \Delta)u_f + \Delta u_{ff}] \\ &= \frac{(1 - \Delta)}{(1 + \Delta)} u_{ff} + \frac{2(\Delta - 1)}{\Delta} u_f + \frac{2}{\Delta(1 + \Delta)} u_w, \quad \text{for } \Delta \geq \frac{1}{2}. \end{aligned}$$

This treatment helps to improve the accuracy in the velocity approximation when $u(x, t)$ is not well resolved near the wall. Finally, it is easily seen that the present boundary condition treatment can be extended to 3-D flow problems involving curved geometry. The efficacy of such an extension will be examined elsewhere.

3. Results and Discussions. For the proposed boundary condition treatment to be useful, several issues need to be addressed: spatial and temporal accuracy, ability to handle geometric singularity, and the flexibility to handle complex geometry. Channel flows with constant and sinusoidally oscillating pressure gradients with analytic solutions are used to assess the spatial and temporal accuracy. The Stokes first problem (*i.e.*, the flow due to an impulsively started wall) allows one to examine the response of the computed flow field to an imposed singular acceleration. The standard lid-driven cavity flow has a bounded domain but possesses stress or vorticity singularities near the corners between the moving and stationary walls. Finally, flow over a column of circular cylinders is the case used to assess the impact of the boundary treatment on the accuracy of the flow field around a curved boundary.

3.1. Pressure driven channel flows. At steady flow, the exact solution for the x -velocity profile is given by

$$(3.1) \quad u_0(y) = \frac{1}{2} \frac{dp}{dx} \frac{H^2}{\rho\nu} \eta(1 - \eta), \quad 0 \leq \eta \leq 1,$$

where $H = (N_y - 3 + 2\Delta)$ and $\eta = y/H = (j - 2 + \Delta)/H$. To assess the computational error of the LBE solution of the velocity, $u(y)$, the following relative L_2 -norm error is defined

$$(3.2) \quad E_2 = \frac{\left\{ \int_0^H [u(y) - u_0(y)]^2 dy \right\}^{1/2}}{\left\{ \int_0^H u_0^2(y) dy \right\}^{1/2}}.$$

With the oscillating pressure gradient, $\frac{dp}{dx} = Be^{-i\omega t}$, the exact solution can be easily expressed in complex variables. An important parameter in this flow is the Stokes number St defined as,

$$(3.3) \quad St = \frac{H}{\sqrt{\nu/\omega}}.$$

The Stokes number is the ratio of the channel height H to the thickness of the Stokes layer $\sqrt{\nu/\omega}$. Since the error can vary with time, a time average over one period ($T = 2\pi/\omega$) is needed and the relative error is

$$(3.4) \quad E_2 = \frac{\left\{ \int_0^T \int_0^H [u(y, t) - u_0(y, t)]^2 dy dt \right\}^{1/2}}{\left\{ \int_0^T \int_0^H u_0^2(y, t) dy dt \right\}^{1/2}}.$$

In the lattice BGK model, $\delta_t = \delta_x = \delta_y = 1$. Comparing with the channel height $H = (N_y - 3 + 2\Delta)$, the dimensionless grid size (or grid resolution) is H .

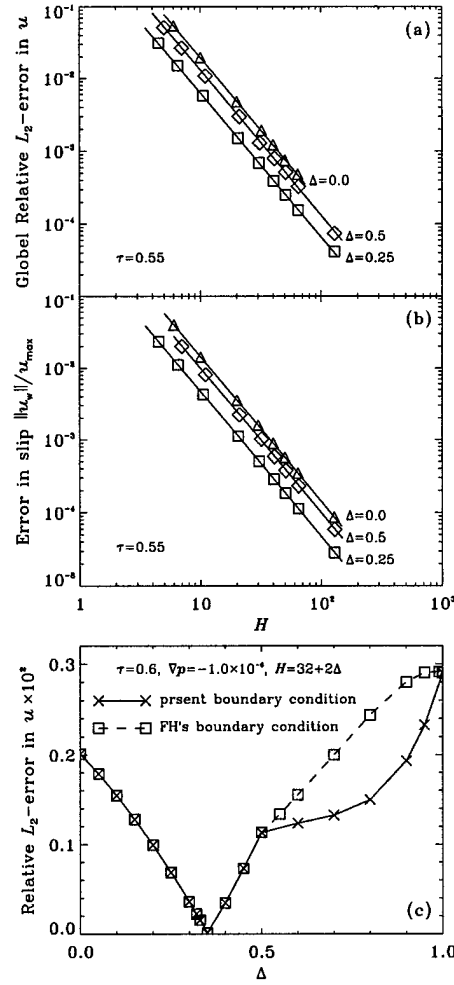


FIG. 6. Convergence of the 2-D steady state pressure-driven channel flow simulations using the present boundary condition. The symbols represent numerical results and the straight lines are the least-square fit of the data. (a) Convergence of global relative L_2 -norm error in $u(y)$ on $H = (N_y - 3 + 2\Delta)$. (b) Quadratic convergence of the slip velocity at wall u_w . (c) Relative L_2 -norm error in $u(y)$ as a function of Δ .

Figure 6(a) shows the dependence of the relative L_2 -norm error on the channel height H for $\tau = 0.55$ and $\Delta = 0.0, 0.25$ and 0.5 . A maximum value of $N_y = 131$ is used. The second-order accuracy is demonstrated in the range of H investigated. It has been well established that the accuracy of the LBE method for the interior points is of second order. The fact that the overall accuracy is of second order in the present case means that the accuracy in the boundary condition is at least of second order. It is worth to note that the derivation given in Section 2 ensures that f_α is second order accurate near the wall. It does not guarantee the second order accuracy of the velocity field near the wall. To address this issue, the wall slip velocity, $u_w = u_x(y = 0)$, is evaluated using a second order extrapolation based on $u_x(y = \Delta)$, $u_x(y = 1 + \Delta)$ and $u_x(y = 2 + \Delta)$. Since the true wall velocity in the pressure driven channel flow is zero, the wall slip velocity u_w provides a measure of the accuracy for the treatment of the wall velocity. Fig. 6(b) shows the dependence of u_w , normalized by the centerline velocity $u_{\max} = -(H^2/8\rho\nu)(dp/dx)$, on H for $\Delta = 0.0, 0.25$, and 0.5 with $\tau = 0.55$. Quadratic convergence is clearly observed in all three cases which demonstrate the second

order accuracy of the velocity field near the solid wall. This is entirely consistent with the results shown in Fig. 6(a) which involves global convergence rather than the local ($y = 0$) convergence. Fig. 6(c) shows the relative error as a function of Δ using the present boundary treatment [Eqs. (2.3), (2.4), (2.13), (2.18), and (2.21)] for $0 \leq \Delta \leq 1$. The error in the range of $0 \leq \Delta \leq 1/2$ is comparable to those in the range of $1/2 < \Delta \leq 1$. The present boundary condition treatment does not induce larger computational error and is substantially more robust. Furthermore the 2nd-order accuracy is achieved in general by the present treatment for $\Delta \leq 1/2$.

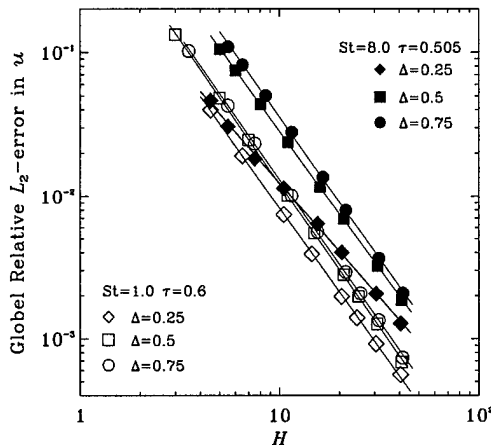


FIG. 7. Dependence of the L_2 -norm error in $u(y)/u_{\max}$ on the lattice resolution $H = (N_y - 3 + 2\Delta)$ in oscillating pressure driven channel flow. Stokes number $St = H/\sqrt{\nu/\omega} = 1$ and 8. The symbols represent numerical results and the straight lines are the least-square fit of the data.

Figure 7 shows the dependence of the relative L_2 -norm error on the channel height H in the oscillating pressure driven channel flow for Stokes number $St = H\sqrt{\omega/\nu} = 1$ and 8. For $St = 1$, the Stokes layer is as thick as the channel height H . For $\Delta = 0.25, 0.5$, and 0.75 , second-order accuracy in space is clearly demonstrated. Since the time step δ_t in LBE is equal to the spatial resolution δ_x , the accuracy in time must also be of second-order in order for the time-averaged L_2 -norm error to have a slope of 2.0 in Fig. 7. For $St = 8$, the Stokes layer thickness is about $1/8$ of the channel height so that the computational error due to the insufficient resolution of the Stokes layer is a significant part of the error. For $\Delta = 0.25$, the first lattice in the flow field is only a quarter of the lattice size away from the wall. The Stokes layer is thus better resolved for $\Delta = 0.25$ (denoted by solid circles in Fig. 7) than for $\Delta = 0.5$ and 0.75 . However, as H increases, the difference between $\Delta = 0.25$ and $\Delta = 0.5$ and 0.75 becomes smaller since all have reasonable resolutions in the Stokes layer. Although the slope for the error curve for $\Delta = 0.25$ is observed to be about 1.5 that is less than 2, it is an indication of the better-than-expected accuracy at the low resolution end.

3.2. Stokes first problem: Flow due to an impulsively started wall. For a wall located at $y = 0$ that is impulsively started, an unsteady Stokes layer of thickness $O(\sqrt{\nu t})$ develops near the wall. For a fixed-grid computation, the error at small time is expected to be large due to insufficient spatial resolution. In the LBE method, this is also compounded by the use of fixed δ_t ($= \delta_x = \delta_y = 1$). Figure 8 shows the velocity profiles at $t = 100$ (in lattice unit). The wall velocity is $U = 0.1$ in lattice unit. The relaxation time $\tau = 0.52$ gives kinematic viscosity $\nu = 0.0067$. Similar to the oscillating pressure driven channel flow, the error is smaller for $\Delta = 0.25$ than for $\Delta = 0.5$ and 0.75 due to a better spatial resolution near the wall.

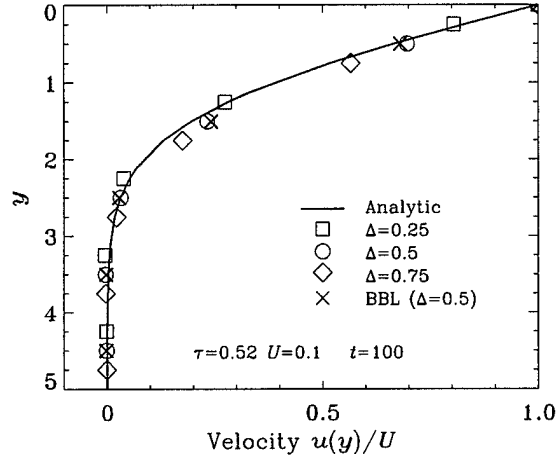


FIG. 8. Velocity profiles $u(y, t)/U$ of an impulsively started plate (Stocks first problem) with $\Delta = 0.25, 0.5$, and 0.75 (symbols), at $t = 100$ (in lattice unit). The solid line represents the exact solution of the problem. The bounce back on the link (BBL) always sets $\Delta = 0.5$.

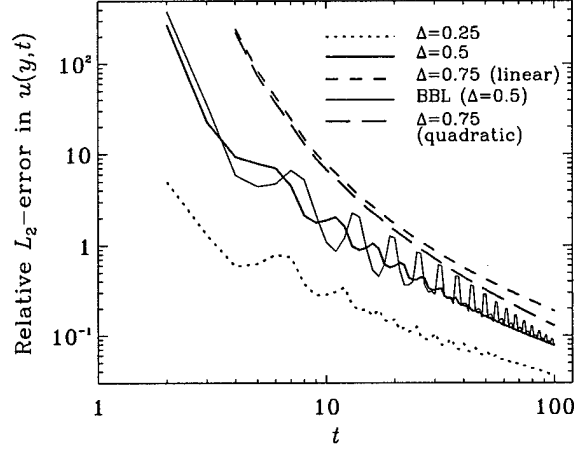


FIG. 9. Relative L_2 -norm error of the velocity profile $u(y, t)$ during the initial transient of the impulsively started plate with various values of Δ (0.25, 0.5, and 0.75). The "linear" version of the boundary condition corresponds to Eq. (2.13). The "quadratic" version corresponds to Eq. (2.22). BBL is limited to $\Delta = 0.5$ only.

Figure 9 shows the temporal variation of the relative L_2 -norm error defined as

$$(3.5) \quad E_2(t) = \frac{\left\{ \int_0^H [u(y, t) - u_0(y, t)]^2 dy \right\}^{1/2}}{\left\{ \int_0^H u_0^2(y, t) dy \right\}^{1/2}},$$

for $\Delta = 0.25, 0.5$, and 0.75 . The result using the standard bounce-back on the link (BBL) scheme, which always sets $\Delta = 0.5$, is also shown. The large relative errors in the beginning are due to the smaller values of the denominator in the above equation. It should be emphasized that this flow at small time is difficult to deal with for any computational technique due to the singular acceleration and large spatial gradient. For an impulsively started Couette flow, the long-time solution approaches the exact linear velocity profile

because the LBE method is a second-order accurate one. It is interesting to note that the present boundary condition treatment for $\Delta = 0.5$ gives a slightly smaller error than the BBL scheme in this highly transient case. In such a transient flow, the computational accuracy in the near-wall region is typically dictated by the near-wall spatial resolution which must be smaller than the Stokes layer thickness in order to resolve the local flow field. In a finite difference calculation for such a flow, δ_t and δ_x can be independently chosen. If δ_x is not sufficiently small, further reduction in δ_t will not lead to improvement in accuracy. At small t , neither the BBL scheme nor the present treatment resolved the Stokes layer so that the error is large. After the Stokes layer grows to certain thickness, the spatial resolution becomes adequate and the accuracy then improves. In view of the “slow flow” condition (2.5) introduced in the derivation, the performance of the current boundary treatment is comparable or better than the conventional bounce-back on the link scheme.

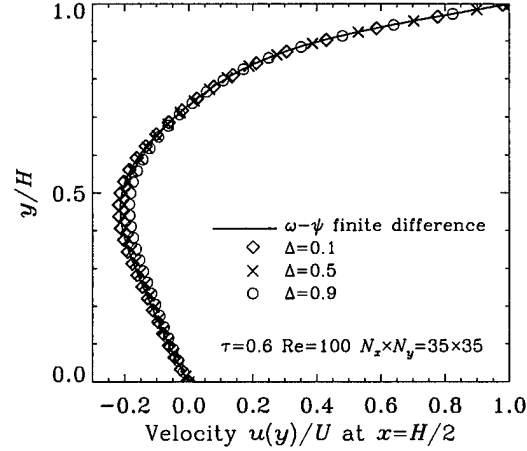


FIG. 10. Velocity profiles at the center ($x/H = 1/2$) in lid-driven cavity flow with various values of Δ (0.1, 0.5, and 0.9) at $Re = 100$.

3.3. Flow in a lid-driven square cavity. Figure 10 shows the velocity profiles at the center ($x/H = 1/2$) of the cavity of width H at $Re = 100$ with $\tau = 0.6$. Only 35×35 lattices are used and the cavity width is $H = (N_x - 3 + 2\Delta) = 32 + 2\Delta$. This requires the lid velocity to be $U = \nu Re/H = 3.33/H$ in the lattice unit. It has a negligible compressibility effect for $H \sim 32$. A well-resolved finite difference solution for the velocity field based on the stream function-vorticity formulation is also shown for comparison. The velocity profile with $\Delta = 0.1$ agrees well the finite difference solution. For $\Delta = 0.5$, the result is rather reasonable with such a resolution. The difference is slightly larger on the negative velocity part for $\Delta = 0.9$. The corner singularity in stress (or vorticity) is well handled for $\tau = 0.6$ and $N_x = 35$. However for τ close to 0.5 and with $N_x = 35$, the corner singularity induces wiggles in the velocity field. This issue will be examined elsewhere. Flow field for $Re = 1000$ is obtained with 67×67 lattices using $\Delta = 0.1, 0.5$, and 0.9 . Similar behavior in the velocity profiles is observed.

3.4. Uniform flow over a column of circular cylinders. To simulate the external flow over a single cylinder would require placing the outer boundary far away from the cylinder. In order to keep the computational effort at a reasonable level in using constant space lattices, a column of circular cylinders of radius r and center-to-center distance H is considered instead. The flow field that needs to be computed is thus limited to $-H \leq y \leq H$. At $y = -H$, the lattice is $j = 2$. The boundary conditions at $j = 1$ for f_α 's

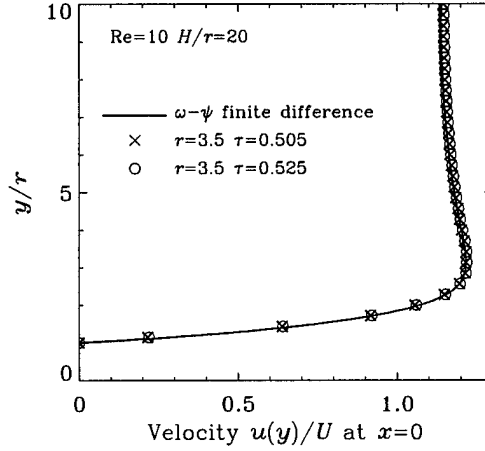


FIG. 11. Flow past a column of cylinders. Velocity profiles at $x = 0$ for uniform flow over a column of cylinders. The cylinder has a diameter ($2r$) of 7 lattice units. The cylinder center-to-center distance $H = 70$ in lattice units.

are given by the following symmetry properties,

$$(3.6) \quad \begin{aligned} f_0(i, 1) &= f_0(i, 3), & f_1(i, 1) &= f_1(i, 3), & f_2(i, 1) &= f_8(i, 3), \\ f_3(i, 1) &= f_7(i, 3), & f_4(i, 1) &= f_6(i, 3), & f_5(i, 1) &= f_5(i, 3), \\ f_6(i, 1) &= f_4(i, 3), & f_7(i, 1) &= f_3(i, 3), & f_8(i, 1) &= f_2(i, 3). \end{aligned}$$

Similar conditions hold at $y = H$ for $j = N_y$. At the inlet, the uniform velocity, $u(y) = U$, is specified at $i = 1.5$. Using $\Delta = 0.5$, $\chi = 0$, Eq. (2.3) is applied to obtain f_α 's at $i = 1$. At the exit, a simple extrapolation is used,

$$(3.7) \quad f_\alpha(N_x, j) = 2f_\alpha(N_x - 1, j) - f_\alpha(N_x - 2, j), \quad \text{for } \alpha = 4, 5, \text{ and } 6.$$

On the surface of the circular cylinder, Eqs. (2.3), (2.4), (2.13), (2.18), and (2.21) proposed in this paper are used to update the boundary conditions for f_α 's.

Figure 11 shows the velocity profile $u(x = 0, y)/U$ for $H/r = 20$ at $Re = 2U\tau/\nu = 10$ using $r = 3.5$. Two values of relaxation time τ , 0.505 and 0.525, are used. For $r = 3.5$, there are only 7 lattices from the front to the back stagnation points. The finite difference solution is obtained using ω - ψ formulation with body-fitted coordinates [26] and over 200 grid points are distributed along the upper half of the circle. These two solution with $\tau = 0.505$ and $\tau = 0.525$ are virtually identical to each other and they are both close to the finite difference solution. Fig. 12 shows the centerline ($y = 0$) velocity variations, upstream and downstream, at $Re = 10$ and 40. The sharp gradient near the front stagnation point, the length of the separation bubble, the maximum of the separation bubble velocity, and the recovery of the wake velocity are all in excellent agreement with the well resolved finite difference solution.

As can be seen now that an important improvement of the present boundary condition treatment over the bounce-back scheme is that it can preserve the accuracy of the geometry under consideration. To further demonstrate this point, consider flow over a circular cylinder of radius r with the coordinate centered at the center of the cylinder. For $r = 3.4$ and 3.8, the front stagnation points are located at $x = -3.4$ and -3.8 , respectively. With the bounce-back on the link (BBL) scheme, the front stagnation points in both cases will be placed at $x = -3.5$ which is half-way between the lattice at $x = -4$ and $x = -3$ on the centerline. In the present method, $\Delta = 0.6$ and 0.2 for $r = 3.4$ and 3.8, respectively. The difference in Δ can be accurately

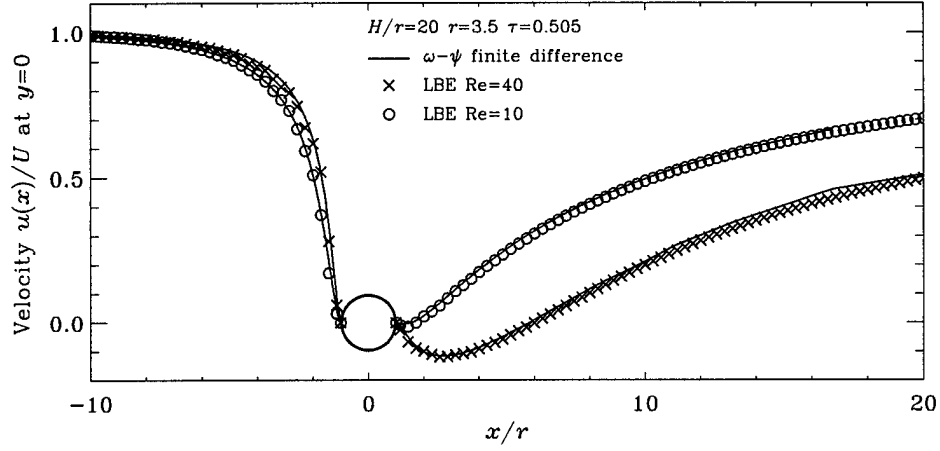


FIG. 12. Flow past a column of cylinders. Centerline ($y = 0$) velocity variation for a uniform flow over a column of cylinders for $Re = 10$ and 40 . The cylinder diameter $2r$ is only of 7 lattice units. Finite difference results are based on ω - ψ formulation and are well resolved.

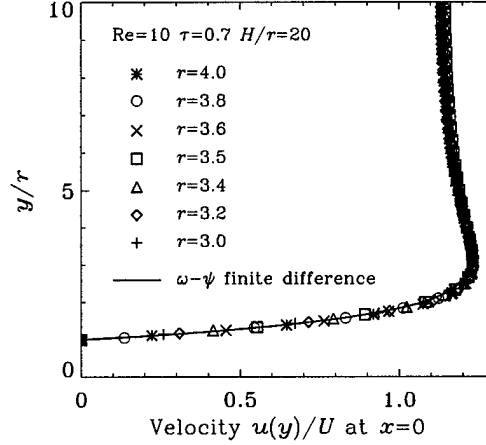


FIG. 13. Flow past a 2-D cylinder. Similar to FIG. 11. Comparison of the velocity profiles at $x = 0$ for the radius $r = 3.0, 3.2, 3.4, 3.5, 3.6, 3.8$ and 4.0 with $Re = 10$, $\tau = 0.7$, and $H/r = 20$.

incorporated in the evaluation of $\tilde{f}_{\alpha}(x_b, t)$. This implies that although the boundary links for $r = 3.4$ will be different from those for $r = 3.8$, the flow fields based on $r = 3.4$ and $r = 3.8$ should be nearly the same when the coordinates are normalized by the radius r . To validate this point, a series of computations are carried out for $r = 3.0, 3.2, 3.4, 3.5, 3.6, 3.8$ and 4.0 for $H/r = 20$ at $Re = 10$. The profiles of the dimensionless x -component velocity $u_x(x, y)/U$ as a function of y/r at $x = 0$ are compared for these seven different radii r in Fig. 13. Excellent agreement is observed. Figure 14 compares the $u_x(x, y)/U$ as a function of x/r at $y = 0$ for both the downstream and upstream regions for these seven different radii. Again, all seven cases compare very well even in the near wall region. Furthermore, the LBE solutions with different radii and the same Reynolds number all well agree with the $\omega - \phi$ finite difference solution of the incompressible NS equation with a well resolved resolution. This clearly demonstrates that the present boundary condition treatment has maintained geometric fidelity even with coarse grid resolutions.

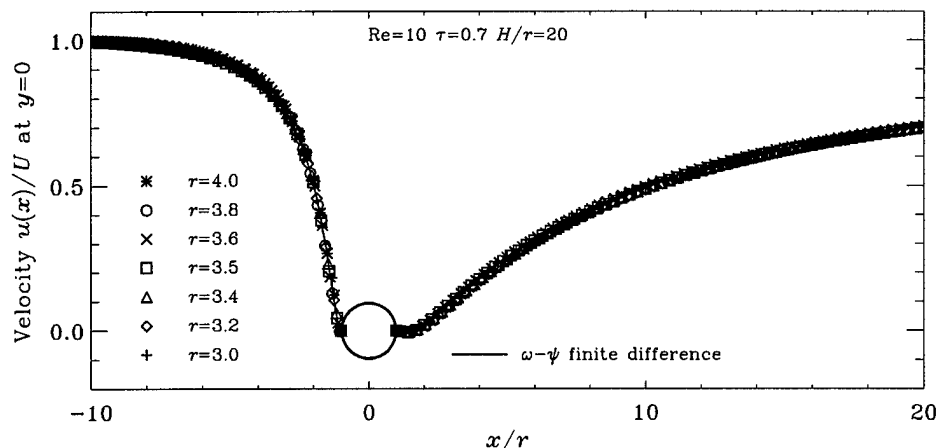


FIG. 14. Flow past a 2-D cylinder. Similar to FIG. 12. Comparison of the centerline ($y = 0$) velocity for radius $r = 3.0, 3.2, 3.4, 3.5, 3.6, 3.8$ and 4.0 with $Re = 10$, $\tau = 0.7$, and $H/r = 20$.

It is noted that the interpolation for $\tilde{f}_{\alpha}(\mathbf{x}_b, t)$ given by Eq. (2.3) is carried along the line in the direction of \mathbf{e}_{α} . The results for flow over a cylinder are quite satisfactory. Other interpolation procedures can certainly be devised to use more information on neighboring lattices in the flow field. However, this will result in a lot more complications in the implementation. It is not clear if such an attempt will necessarily lead to further improvement over the present approach.

4. Conclusion. In this work a second-order accurate boundary condition treatment for the lattice Boltzmann equation is proposed. A series of studies are conducted to systematically validate the accuracy and examine the robustness of the proposed boundary condition in steady and unsteady flows involving flat and curved walls. Compared with the existing method for treating boundary condition in the lattice Boltzmann method, the proposed treatment has the following advantages. (i) It can preserve the geometry of interest without truncating it into a series of stair steps. (ii) The boundary treatment generally results in solutions of second-order accuracy for the velocity field in space, and in time for some cases. (iii) Compared with the widely used bounce-back on the link scheme, the present treatment gives comparable or better results for the flow field under otherwise identical computational parameters.

Acknowledgments. This work is supported by NASA Langley Research Center under the program of Innovative Algorithms for Aerospace Engineering Analysis and Optimization. R. Mei also acknowledges partial support of Alcoa Foundation, the Engineering Research Center (ERC) for Particle Science and Technology at the University of Florida, the National Science Foundation (EEC-9402989), and Industrial partners of the ERC. W. Shyy acknowledges partial support of AFOSR and Eglin AFB. The authors are grateful to Dr. O. Filippova and Prof. D. Hänel for helpful discussions.

REFERENCES

- [1] T. ABE, *Derivation of the lattice Boltzmann method by means of the discrete ordinate method for the Boltzmann equation*, J. Comp. Phys., 131 (1997), pp. 241–246.
- [2] O. BEHREND, *Solid boundaries in particle suspension simulations via lattice Boltzmann method*, Phys. Rev. E, 52 (1995), pp. 1164–1175.

- [3] R. BENZI, S. SUCCI, AND M. VERGASSOLA, *The lattice Boltzmann equation: Theory and applications*, Phys. Rep., 222 (1992), pp. 145–197.
- [4] P.L. BHATNAGAR, E.P. GROSS, AND M. KROOK, *A model for collision processes in gases. I. Small amplitude processes in charged and neutral one-component system*, Phys. Rev. A, 94 (1954), pp. 511–525.
- [5] H. CHEN, S. CHEN, AND W.H. MATTHAEUS, *Recovery of the Navier-Stokes equations using a lattice gas Boltzmann method*, Phys. Rev. A, 45 (1992), pp. R5339–R5342.
- [6] S. CHEN AND G.D. DOOLEN, *Lattice Boltzmann method for fluid flows*, Ann. Rev. Fluid Mech., 30 (1998), pp. 329–364.
- [7] S. CHEN, D. MARTINEZ, AND R. MEI, *On boundary conditions in lattice Boltzmann method*, Phys. Fluids, 8 (1996), pp. 2527–2536.
- [8] O. FILIPPOVA AND D. HÄNEL, *Grid refinement for lattice-BGK models*, J. Comp. Phys., 147 (1998), pp. 219–228.
- [9] C.A.J. FLETCH, *Computational Techniques for Fluid Dynamics*, Vols. I & II, Springer-Verlag, New York, 1988.
- [10] U. FRISCH, B. HASSLACHER, AND Y. POMEAU, *Lattice-gas automata for the Navier-Stokes equation*, Phys. Rev. Lett., 56 (1986), pp. 1505–1508.
- [11] I. GINZBOURG AND P.M. ALDER, *Boundary flow condition analysis for the three-dimensional lattice Boltzmann model*, J. Phys. II France, 4 (1994), pp. 191–214.
- [12] I. GINZBOURG AND D. D'HUMIÈRES, *Local second-order boundary methods for lattice Boltzmann models*, J. Stat. Phys., 84 (1996), pp. 927–971.
- [13] X. HE AND G. DOOLEN, *Lattice Boltzmann method on curvilinear coordinates system: Flow around a circular cylinder*, J. Comp. Phys., 134 (1997), pp. 306–315.
- [14] X. HE AND L.-S. LUO, *A priori derivation of the lattice Boltzmann equation*, Phys. Rev. E, 55 (1997), pp. R6333–R6336.
- [15] ———, *Theory of the lattice Boltzmann method: From the Boltzmann equation to the lattice Boltzmann equation*, Phys. Rev. E, 56 (1997), pp. 6811–6817.
- [16] ———, *Lattice Boltzmann model for the incompressible Navier-Stokes equation*, J. Stat. Phys., 88 (1997), pp. 927–944.
- [17] X. HE, L.-S. LUO, AND M. DEMBO, *Some progress in lattice Boltzmann method. Part I. Nonuniform mesh grids*, J. Comp. Phys., 129 (1996), pp. 357–363.
- [18] ———, *Some progress in lattice Boltzmann method. Reynolds number enhancement in simulations*, Physica A, 239 (1997), pp. 276–285.
- [19] X. HE, Q. ZOU, L.-S. LUO, AND M. DEMBO, *Analytic solutions and analysis on non-slip boundary condition for the lattice Boltzmann BGK model*, J. Stat. Phys., 87 (1997), pp. 115–136.
- [20] F. HIGUERA, S. SUCCI, AND R. BENZI, *Lattice gas dynamics with enhanced collisions*, Europhys. Lett., 9 (1989), pp. 345–349.
- [21] A.J.C. LADD, *Numerical simulation of particulate suspensions via a discretized Boltzmann equation. Part 2. Numerical results*, J. Fluid Mech. 271 (1994), pp. 311–339.
- [22] L.-S. LUO, *Analytic solutions of linearized lattice Boltzmann equation for simple flows*, J. Stat. Phys., 88 (1997), pp. 913–926.
- [23] ———, *Unified theory of the lattice Boltzmann models for non-ideal gases*, Phys. Rev. Lett., 81 (1998), pp. 1618–1621.

- [24] G. MCNAMARA AND G. ZANETTI, *Use of the Boltzmann equation to simulate lattice-gas automata*, Phys. Rev. Lett., 61 (1988), pp. 2332–2335.
- [25] R. MEI AND W. SHYY, *On the finite difference-based lattice Boltzmann method in curvilinear coordinates*, J. Comp. Phys., 143 (1998), pp. 426–448.
- [26] R. MEI, J. XIONG, AND R. TRAN-SON-TAY, *Motion of a sphere oscillating at low Reynolds numbers in a visco-elastic-fluid-filled cylindrical tube*, J. Non-Newtonian Fluid Mech., 66 (1996), pp. 169–192.
- [27] D. R. NOBLE, S. CHEN, J. G. GEORGIADIS, AND R. O. BUCKIUS, *A consistent hydrodynamic boundary condition for the lattice Boltzmann method*, Phys. Fluid, 7 (1995), pp. 203–209.
- [28] R. PEYRET AND T. D. TAYLOR, *Computational Technique for Fluid Dynamics*, Vol. II, Springer-Verlag, New York, 1983.
- [29] Y. H. QIAN, D. D'HUMIÈRES, AND P. LALLEMAND, *Lattice BGK models for Navier-Stokes equation*, Europhys. Lett., 17 (1992), pp. 479–484.
- [30] D. H. ROTHMAN AND S. ZALESKI, *Lattice-Gas Cellular Automata: Simple Models of Complex Hydrodynamics*, Cambridge University Press, New York, 1997.
- [31] W. SHYY, *Computational Modeling for Fluid Flow and Interfacial Transport*, Corrected printing, Elsevier, Amsterdam, 1997.
- [32] D. P. ZIEGLER, *Boundary conditions for lattice Boltzmann simulations*, J. Stat. Phys., 71 (1993), pp. 1171–1177.
- [33] Q. ZOU AND X. HE, *On pressure and velocity boundary conditions for the lattice Boltzmann BGK model*, Phys. Fluids, 9 (1997), pp. 1591–1598.